
Chapter 5. Modelling of the GPR radar range equation in the time domain

5.1. Introduction

For a time domain GPR, a time domain representation is an obvious choice. It allows a compact and more accurate description of the system performances. Therefore we will model in this chapter the radar range equation in the time domain.

Describing performances of a time domain GPR system, using the radar range equation has mainly three drawbacks:

1. The radar range equation contains frequency dependent terms, hence they have to be expressed over the whole frequency band of interest. As time domain systems have intrinsically a large bandwidth, describing the system performance with the frequency dependent parameters is complicated
2. The radar range equation does not specify the nature of the transmitted signal
3. For a time domain system it is more practical to express the minimum detectable signal in terms of peak voltages and/or signal shapes instead of signal power only.

In the previous chapter we explained how time domain antennas can be characterised by their normalised impulse response. By considering the antenna as a convolution operator, we get a mechanism for modelling a whole radar system as a cascade of linear responses, which will lead in this chapter to a time domain equivalence of the radar range equation. Furthermore some modifications will be introduced to adapt the radar equation to the application of the GPR. Each term of the radar range equation in the time domain will be discussed in detail.

5.2. Radar range equation

The radar range equation is a useful description of the factors influencing radar performance. It gives the received power at the radar system in terms of the radar characteristics, the illuminated target and the frequency. The basic equation for a monostatic radar in free space illuminating a point scatterer is given by [1]

$$P_r(f) = \frac{P_t(f)G_t(f)}{4\pi R^2} \frac{\mathbf{s}(f)}{4\pi R^2} A_e(f) \quad (5.1)$$

with

$P_r(f)$: the received signal power

$P_t(f)$: the transmitted signal power

$G_t(f)$: the maximum gain of the transmitting antenna

R : the radar-to-target distance

$\mathbf{s}(f)$: the radar cross section of the target

$A_e(f)$: the effective aperture area of receiving antenna.

The effective aperture of an antenna is related to the gain and the wavelength by

$$A_e(f) = \frac{G(f)\lambda^2}{4\pi} \quad (5.2)$$

Hence the monostatic radar range equation can be written as

$$P_r(f) = \frac{P_t(f)G^2(f)I^2\mathbf{s}(f)}{(4\mathbf{p})^3 R^4} \quad (5.3)$$

The Radar Cross Section (RCS) $\mathbf{s}(f)$, expressed in square meters, is a measure of the equivalent surface area of a target that is seen by the radar [2]. In the definition of the RCS it is assumed that the target is in free space and in the far field of the radar. In a bistatic configuration the RCS of a target will be function of the direction of the incoming field on the target and of the direction towards the receiving antenna, therefore it should be expressed as a function of both incident and scattering angle. The bistatic RCS is mathematically expressed as

$$\mathbf{s}_b(\mathbf{q}, \mathbf{j}; \mathbf{q}', \mathbf{j}') = 4\mathbf{p} \lim_{R \rightarrow \infty} R^2 \frac{|E_s(\mathbf{q}', \mathbf{j}')|^2}{|E_i(\mathbf{q}, \mathbf{j})|^2} \quad (5.4)$$

where

E_s : the scattered field at the receiver

E_i : the incident field on the target

The term $4\mathbf{p}R^2$ is to factor out the spreading loss. The angles \mathbf{q} and \mathbf{j} define the direction of propagation of the incident field and the angles \mathbf{q}' and \mathbf{j}' the direction of the scattered field. In the most general case the RCS must also be expressed as a function of the polarisation of the incident and scattered field.

5.3. GPR range equation

The GPR system performance is also governed by the radar range equation, but some modifications have to be made. For instance, in the case of a GPR, the transmitting and receiving antennas are physically two separated antennas. Normally the antennas are close to each other, but as the object can be in the neighbourhood of the antenna

configuration, it is more correct to adapt expression (5.3) for the bistatic case. This can be done by replacing the range R and the RCS of the target by their corresponding bistatic quantities. These corrections are not that important and can, in some cases, be omitted. More important is the introduction of some additional losses, *i.e.* the transmission loss at the air-ground interface, transmission losses associated with any mismatch in the ground (different layers in the ground), propagation loss in the ground and the losses due to an off-boresight position of the target [3]. All these losses are usually introduced in the radar range equation by the factors F_t and F_r , called respectively "the pattern propagation factor for transmitting-antenna-to-target path and target-to-receiving-antenna path". The factor F_t is defined as the ratio of the electric field strength at the target position, to that which would exist at the same distance from the radar in free space and on boresight of the antenna. The factor F_r is analogously defined [1]. Taking into account the pattern propagation factors, the radar range equation for a GPR system becomes

$$P_r(f) = \frac{P_t(f)G_t(f)}{4\pi R_t^2} \frac{\mathbf{s}_b(f)}{4\pi R_r^2} \frac{G_r(f)I^2}{4\pi} F_t^2 F_r^2 \quad (5.5)$$

with

$G_r(f)$: the maximum gain of the receiving antenna

R_t : the distance from transmitting antenna to the target

R_r : the distance from receiving antenna to the target

$\mathbf{s}_b(f)$: the bistatic radar cross section of the target

$F_t(f)$: the pattern propagation factor for transmitting-antenna-to-target path

$F_r(f)$: the pattern propagation factor for target-to-receiving-antenna path.

When the GPR is used for relatively small depths, like in the demining application, we can assume constant ground characteristics and no multiple layers between the air-ground interface and the target. In this case the pattern propagation factors F_t^2 and

F_r^2 can be split into 4 parts: the transmission loss at the air-ground interface, the retransmission loss for the backscattered signal at the ground-air interface, the two-way propagation losses in the ground, and the off-boresight position of the target.

The transmission power loss L_{a-g} at the air-ground interface and the retransmission power loss L_{g-a} at the ground-air are given by

$$L_{a-g} = \frac{Z_{ground}}{Z_0} \left| \frac{2Z_{ground}}{Z_{ground} + Z_0} \right|^2 \quad \text{and} \quad L_{g-a} = \frac{Z_0}{Z_{ground}} \left| \frac{2Z_0}{Z_{ground} + Z_0} \right|^2 \quad (5.6)$$

where Z_{ground} is the complex characteristic impedance of the ground, given by

$$Z_{ground} = \sqrt{\mathbf{m}/\mathbf{e}^*} \approx \sqrt{\mathbf{m}} / \sqrt{\mathbf{e}'(1 - j \tan \mathbf{d})}$$

The two-way propagation losses in the ground is given by

$$e^{-2\mathbf{a}(R_{t,ground} + R_{r,ground})} \quad (5.7)$$

with \mathbf{a} : the attenuation constant of the ground as defined in (2.20)

$R_{t,ground}$ and $R_{r,ground}$: the parts of the one-way path length in the ground.

5.4. Radar range equation in the time domain

In this section, we develop an equivalent radar range equation in the time domain [4]. To make the difference with the conventional radar range equation of (5.5), we denote it as *the time domain radar range equation*. In a first step, the basic time domain equation for a radar in free space is developed. Therefore, we will characterise the antennas by their normalised impulse response, integrating all frequency dependent

antenna characteristics. One of the advantages of considering the UWB antenna as a convolution operator is that we get a mechanism for expressing the radar range equation as a cascade of linear responses.

Consider an electromagnetic configuration as shown in Fig. 5-1. The origin for the coordinates is taken in the virtual source of the transmitting antenna. We define

$\vec{a}_i = \frac{\vec{r}'}{|\vec{r}'|}$ as the direction of radiation of the transmitting antenna towards the target located at co-ordinate \vec{r}' . It is the incident direction of the field, from the point of view of the target.

$\vec{a}_s = \frac{\vec{r}'' - \vec{r}'}{|\vec{r}'' - \vec{r}'|}$ as the direction of the scattered field from the target towards the receiving antenna. The virtual source of the receiving antenna is located at \vec{r}'' .

When using the normalised impulse response of the antenna, the radiated field in the point \vec{r}' in the far field is given by (4.14). This field will be the incoming field for the target and is expressed as

$$\frac{E_{inc}(\vec{r}', t)}{\sqrt{Z_0}} = \frac{1}{2\mathbf{p}|r'|c} h_{N,Tx}(\vec{a}_i, t) \otimes \frac{1}{\sqrt{Z_c}} \frac{dV_s(t - |r'|/c)}{dt} \quad (5.8)$$

where $h_{N,Tx}(\vec{a}_i, t)$ is the normalised impulse response of the transmitting antenna in the direction \vec{a}_i , V_s is the excitation voltage at the antenna feed, Z_c the impedance of the feed cable, and $Z_0 = 120\mathbf{p}$.

We define the Impulse Response (IR) $\Lambda_{1,1}(\vec{a}_i, \vec{a}_s, t)$ of a given target so that the scattered field in a point \vec{r}'' can be described as

$$E_{scat}(\vec{r}'', t) = \frac{1}{4\mathbf{p}|\vec{r}'' - \vec{r}'|} \Lambda_{1,1}(\vec{a}_i, \vec{a}_s, t) \otimes E_{inc}(\vec{r}', t - |\vec{r}'' - \vec{r}'|/c) \quad (5.9)$$

The impulse response $\Lambda_{1,1}(\vec{a}_i, \vec{a}_s, t)$ only takes into account the backscattered signal in the same polarisation as the incoming field and is expressed in [m/s]. It can be seen as the time equivalent of the square root of the radar cross section. The factor $1/|\vec{r}'' - \vec{r}'|$ introduce the spreading loss. The impulse response is described in more detail in Section 5.6.4.

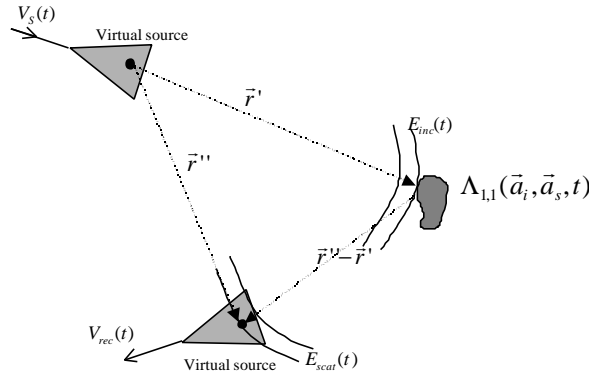


Fig. 5-1: Electromagnetic configuration

The received voltage $V_{rec}(t)$ at the output of the receiving antenna is calculated by (4.15) as

$$\frac{V_{rec}(t)}{\sqrt{Z_c}} = h_{N,Rx}(-\vec{a}_s, t) \otimes \frac{E_{scat}(\vec{r}'', t)}{\sqrt{Z_0}} \quad (5.10)$$

Combining (5.8), (5.9) and (5.10), the basic time domain radar equation for a radar in free space is found as

$$V_{rec}(t) = \frac{1}{8\mathbf{p}^2 R_i R_r c} h_{N,Tx}(\vec{a}_i, t) \otimes \Lambda_{1,1}(\vec{a}_i, \vec{a}_s, t) \otimes h_{N,Rx}(-\vec{a}_s, t) \otimes \frac{dV_s(t)}{dt} \quad (5.11)$$

With $R_t = |\vec{r}|$: the total path length from transmitting antenna to the target

$R_r = |\vec{r}'' - \vec{r}'|$: the total path length from receiving antenna to the target.

Equation (5.11) gives a relation between the excitation voltage (applied at the transmitting antenna) and the received voltage (measured at the receiving antenna) as a cascade of 3 time-invariant linear systems: the transmitting antenna, the target in free space and the receiving antenna, each described by their IR.

Note that in equation (5.11) the total propagation delay $|\vec{r}| + |\vec{r}'' - \vec{r}'|/c$ is omitted for simplicity. If this delay is important for the application, it has to be included in equation (5.11).

If the minimal detectable transient signal of the receiver is known, expression (5.11) can be used to calculate the range performance of the impulse radar system. The capability of an impulse radar system to detect a scattered signal can be termed in system detectability:

$$D = 20 \log \left(\frac{V_{rec, peak}}{V_{s, peak}} \right) \quad (5.12)$$

In general the limiting factor of detectability is the noise performance of the receiver. The received voltage must be larger than the noise voltage generated by the receiver. In some cases the detectability can be also limited by the coupling between the antennas. The pulse, radiated by the transmitting antenna will couple directly into the receiving antenna and will ring down. Normally this coupling can be compensated for. If not, the ringing can interfere with the useful backscattered signal and limit the detectability of the system.

5.5. GPR range equation in the time domain

As for the frequency domain, the time domain radar range equation can be adapted for the GPR. Therefore, expression (5.11) has to be modified to take into account some additional losses. In the scope of demining applications, the antennas are used off-ground, hence we will have to introduce the transmission loss at the air-ground interface and the propagation loss in the ground (Fig. 5-2). The losses due to the off-boresight position of the target are already taken into account by $h_N(\mathbf{q}, \mathbf{j}, t)$, representing the normalised impulse response in the direction (\mathbf{q}, \mathbf{j}) . Suppose that the two-way path loss, due to the propagation in the lossy ground is characterised by an impulse response $g_d(t)$. In the absence of noise, the complete GPR radar range equation in the time domain can then be written as

$$V_{rec}(t) = \frac{T_{a-g} \cdot T_{g-a}}{8p^2 R_t R_r c} g_d(t) \otimes h_{N,Tx}(\bar{\mathbf{a}}_i, t) \otimes \Lambda_{1,1}(\bar{\mathbf{a}}_i, \bar{\mathbf{a}}_s, t) \otimes h_{N,Rx}(-\bar{\mathbf{a}}_s, t) \otimes \frac{dV_s(t)}{dt} \quad (5.13)$$

with

R_t : the total path length from transmitting antenna to the target

R_r : the total path length from receiving antenna to the target

$g_d(t)$: the impulse response representing the two-way path length loss in the ground

T_{a-g} : the transmission coefficient at the air-ground interface (air to ground)

T_{g-a} : the transmission coefficient at the air-ground interface (ground to air).

Equation (5.13) allows for any excitation signal $V_s(t)$ to calculate the received voltage $V_{rec}(t)$ at the receiving antenna as a function of time. Note that, if the excitation signal $V_s(t)$ for the implementation of equation (5.13) is measured by the receiver, the influence of the IR of the receiver is automatically taken into account in the time

domain GPR range equation. In the next section, all the terms in equation (5.13), except for the normalised IRs of the antennas, will be discussed in detail.

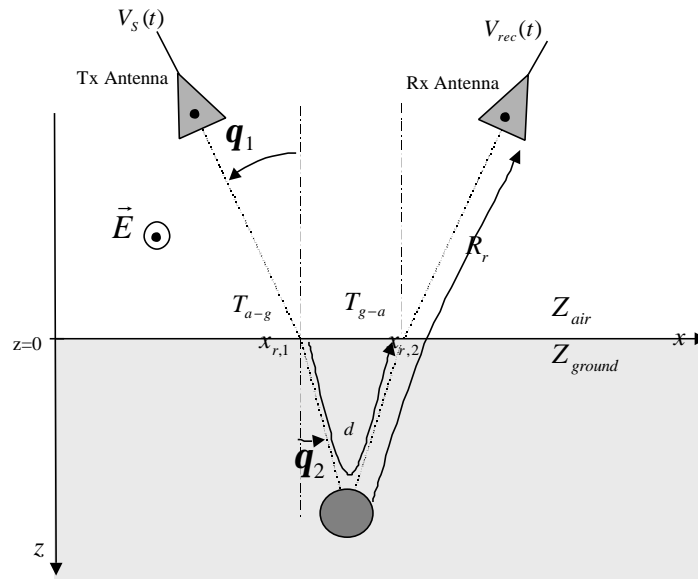


Fig. 5-2: GPR configuration

5.6. Calculation of the different terms in the time domain GPR range equation

5.6.1. Transmission coefficients on the air-ground interface

The reflection and transmission coefficients of a plane wave at the boundary between two isotropic non-conductive media are described by Fresnel's equations [5]. The coefficients are simply function of the relative permeability and permittivity contrasts between the media and of the angle of incidence. For a complete study, two perpendicular polarisations have to be distinguished, *i.e.* the E-field normal to the plane of incidence (cf. Fig. 5-2), called the normal polarisation and the E-field in the plane of incidence, called the parallel polarisation. In general, geological media have a relative permeability equal 1. In this case, the reflection and transmission coefficients at the boundary between two non-conductive geological media are given by

$$\begin{aligned}
 \Gamma_{\perp} &= \frac{\sqrt{\mathbf{e}_1} \cos \mathbf{q}_1 - \sqrt{\mathbf{e}_2} \cos \mathbf{q}_2}{\sqrt{\mathbf{e}_1} \cos \mathbf{q}_1 + \sqrt{\mathbf{e}_2} \cos \mathbf{q}_2} \\
 T_{\perp} &= \frac{2\sqrt{\mathbf{e}_1} \cos \mathbf{q}_1}{\sqrt{\mathbf{e}_1} \cos \mathbf{q}_1 + \sqrt{\mathbf{e}_2} \cos \mathbf{q}_2} \\
 \Gamma_{//} &= \frac{\sqrt{\mathbf{e}_2} \cos \mathbf{q}_1 - \sqrt{\mathbf{e}_1} \cos \mathbf{q}_2}{\sqrt{\mathbf{e}_2} \cos \mathbf{q}_1 + \sqrt{\mathbf{e}_1} \cos \mathbf{q}_2} \\
 T_{//} &= \frac{2\sqrt{\mathbf{e}_1} \cos \mathbf{q}_1}{\sqrt{\mathbf{e}_2} \cos \mathbf{q}_1 + \sqrt{\mathbf{e}_1} \cos \mathbf{q}_2}
 \end{aligned} \tag{5.14}$$

with

$$\sin(\mathbf{q}_2) = \sqrt{\frac{\mathbf{e}_1}{\mathbf{e}_2}} \sin(\mathbf{q}_1) \tag{5.15}$$

and

- Γ_{\perp} : the reflection coefficient for normal polarisation
- T_{\perp} : the transmission coefficient for normal polarisation
- $\Gamma_{//}$: the reflection coefficient for parallel polarisation
- $T_{//}$: the transmission coefficient for parallel polarisation
- \mathbf{q}_1 : the incident angle
- \mathbf{q}_2 : the refraction angle.

In reality, a geological medium is conductive, hence the reflection and transmission coefficients are complex. At radar frequencies, the conductive geological media can be assumed to be free of electric charges and currents, so that conditions for the electric and magnetic fields at the boundaries of the two media are the same as for the non-conductive media case [6]. Hence by analogy, the reflection and transmission coefficients are also given by expression (5.14), providing that the permittivity \mathbf{e} in (5.14) and (5.15) is replaced by the corresponding complex apparent permittivity \mathbf{e}^* of the conductive media. If the imaginary part of the conductivity \mathbf{s}'' is neglected, the apparent permittivity \mathbf{e}^* is approximately given by (2.13) as

$$\mathbf{e}^* = \mathbf{e}'(1 - j \tan \mathbf{d}) \quad (5.16)$$

In the constant Q model (Section 2.2.3) the loss tangent $\tan \mathbf{d}$ and the real part of the permittivity \mathbf{e}' are considered to be independent of frequency, hence the apparent permittivity \mathbf{e}^* is independent of frequency. In this approximation the reflection and transmission coefficients in (5.14) become independent of frequency. This is an important result, as it means that neither the reflection at a boundary between two conductive media nor the transmission through such boundary will introduce dispersion.

Furthermore, in a study by Lehmann [6], it is stated that for radar frequencies, the reflection and transmission coefficients at boundaries between loss-less media is a good approximation for the reflection and the transmission coefficients for conductive media. The latter has been verified and approved with the soil measurements performed in the scope of the HUDEM project [7]. For example, suppose an interface between air and wet sand with a moisture content of 10% ($\mathbf{e}'_r = 7.18$ and $\tan \mathbf{d} = 0.069$ at 2 GHz). In the case were no losses are assumed ($\tan \mathbf{d} = 0$), the transmission coefficient for normal polarisation is calculated to be 0.5224. If the losses are taken into account, the transmission coefficient for normal polarisation is calculated to be $0.5219 + j*0.0135$, which means a difference of 0.0068 dB.

To summarise, in the time domain radar range equation (5.13), the transmission coefficients on the air-ground interface can be calculated using (5.14), if we replace \mathbf{e}_1 by \mathbf{e}_0 , the permittivity of free space, and \mathbf{e}_2 by \mathbf{e}_2' , the real part of the permittivity of the ground. In our configuration (Fig. 5-2), we only work with the electric field normal to the plane of incidence, hence the transmission coefficients as needed for the time domain radar range equation are given by:

$$T_{a-g} = \frac{2\sqrt{\mathbf{e}_0} \cos \mathbf{q}_1}{\sqrt{\mathbf{e}_0} \cos \mathbf{q}_1 + \sqrt{\mathbf{e}_2'} \cos \mathbf{q}_2} \quad (5.17)$$

$$T_{g-a} = \frac{2\sqrt{\mathbf{e}_2'} \cos \mathbf{q}_2}{\sqrt{\mathbf{e}_2'} \cos \mathbf{q}_2 + \sqrt{\mathbf{e}_0} \cos \mathbf{q}_1} \quad (5.18)$$

Note that the transmission coefficients further suppose that the interface is flat and in the far-field of the antennas. In practice these two assumptions are not always respected.

5.6.2. Total path length in the air and in the ground

In the GPR range equation given in (5.13), the total path length from the transmitting antenna to the target, the total path length from the target to the receiving antenna and the two-way path length in the ground are needed. In all of the discussions made thus far, we did not mention the refraction on the air-ground interface. For a correct calculation of the above path lengths, the refraction has to be taken into account and the refraction points, denoted $x_{r,1}$ and $x_{r,2}$ in Fig. 5-2, on the air-ground interface have to be calculated. Suppose a 2-D configuration as shown in Fig. 5-3. The antenna can move at a fix height h above the air-ground interface, so the antenna position is characterised by only one co-ordinate x . The object in the ground is buried at a depth d at position x_2 . The refraction point x_r can be calculated according to Snell's refraction law, assuming the air-ground interface is flat and in the far-field of the antennas. This leads to a system of three equations that can be solved by means of iteration:

$$\begin{aligned} \sin(\mathbf{q}_2) &= \sqrt{\frac{\mathbf{e}_1}{\mathbf{e}_2}} \sin(\mathbf{q}_1) \\ \tan(\mathbf{q}_1) &= \frac{|x - x_r|}{h} \\ \tan(\mathbf{q}_2) &= \frac{|x_2 - x_r|}{d} \end{aligned} \quad (5.19)$$

An accurate approximation however for the calculation of the refraction points is found in the following method [8]. Suppose the relative permittivity ϵ_2 of the second medium is larger than the relative permittivity ϵ_1 of the first one (this is always the case for the antennas in the air). There are two extreme paths between an antenna and an object in the ground. If $\epsilon_2 \rightarrow \infty$, then the refraction point will be at x_2 . If $\epsilon_2 = \epsilon_1$, the refraction point will be at x_1 . For values of ϵ_2 between those two extremes, the refraction point can be linearly approximated by

$$x_r = x_2 + \sqrt{\frac{\epsilon_1}{\epsilon_2}}(x_1 - x_2) \tag{5.20}$$

This simple approximation is very accurate. In the case of antennas scanning at 25 cm above the air-ground interface and an object buried at 10 cm, the maximum error between the approximated position of the refraction point using (5.20) and the real position, is less than 2 mm. This is shown in Fig. 5-4. The position x of the antenna is represented on the x-axis. The position x_r of the refraction point is represented on the y-axis. The relative permittivity of the ground is taken $\epsilon_2 = 9$ for this calculation. The real refraction point is given in red and the approximated one in blue.

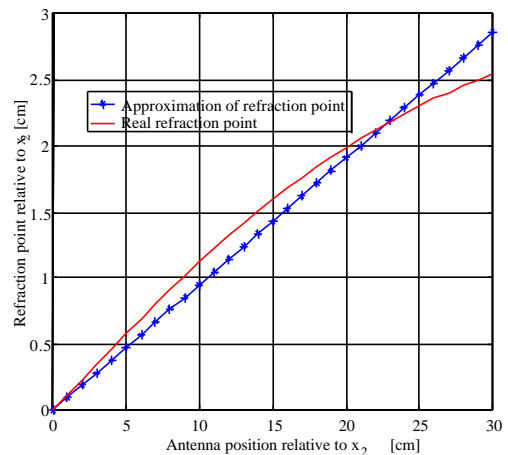
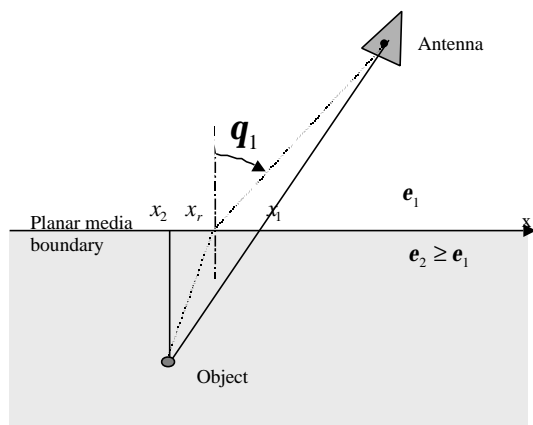


Fig. 5-3: Geometry for the calculation of the refraction point **Fig. 5-4:** Validation of the approximation of the refraction point

In the implementation of the GPR range equation, we use the approximation given by (5.20) to calculate the refraction point on the interface for the path between the transmitting antenna to the target and the refraction point on the interface for the path between the target and the receiving antenna. If the second medium is lossy, the real part of ϵ_2 is used in equation (5.20). Hence the approximated distances R_t , R_r , and d (the total path length in the ground) can be calculated without too much effort.

5.6.3. Ground as a low-pass filter

The propagation losses and dispersion in the ground are not so easy to introduce and need some more explanations. The best way to handle these losses is by representing the ground as a low-pass filter, characterised by its IR $g_d(t)$ or the corresponding Frequency Response Function $G_d(\omega)$. The parameters of this filter are depending on the soil characteristics, *i.e.* the texture of soil, the density and the moisture content, and the two-way path length of the wave in the ground, denoted as d in Fig. 5-2.

As already discussed in Chapter 2, soils are lossy media characterised by a complex conductivity $\sigma' - j\sigma''$ and a complex permittivity $\epsilon' - j\epsilon''$. The solution to Maxwell's equations describing a harmonic plane wave propagating in a lossy medium is given by

$$\vec{E} = \vec{E}_0 e^{-(\vec{a} + j\vec{b})\vec{r}} \quad (5.21)$$

with

$$\mathbf{a} = \omega \sqrt{\mathbf{m}_0 \epsilon'} \sqrt{\frac{1}{2} \cdot (\sqrt{(1 + tg^2 d)} - 1)} \quad \text{the attenuation constant [Np/m] of the medium}$$

$$\mathbf{b} = \omega \sqrt{\mathbf{m}_0 \epsilon'} \sqrt{\frac{1}{2} \cdot (\sqrt{(1 + tg^2 d)} + 1)} \quad \text{the phase constant [rad/m].}$$

According to (5.21), the propagation of the plane wave over a distance d meters in the direction of the propagating wave can be characterised as a linear system with a frequency response function

$$G_d(\mathbf{w}) = e^{-(\mathbf{a}+j\mathbf{b})d} \quad (5.22)$$

Note that the same frequency response function would be found in case of spherical waves, because the spreading loss is already taken into account in the radar equation (5.13).

The constants α and β can be calculated by measuring the complex electrical parameters of the soil over a large frequency band. By an inverse time-frequency transformation or by a filter design method, the impulse response $g_d(t)$, representing the losses of a propagation of d meters in the ground, can be found.

Measuring the electrical parameters over a large bandwidth and designing the filter would be very difficult. Therefore a more convenient way of calculating the filter is presented here. In the constant Q model (Section 2.2.3), the attenuation constant and the phase constant can be approximated by

$$\mathbf{a} = \mathbf{w}\sqrt{\mathbf{m}\mathbf{e}'} \frac{\tan \mathbf{d}}{2} \quad (5.23)$$

$$\mathbf{b} = \mathbf{w}\sqrt{\mathbf{m}\mathbf{e}'} \quad (5.24)$$

with $\tan \mathbf{d}$ small and constant with frequency and \mathbf{e}' constant with frequency. This means that in this approximation \mathbf{a} and \mathbf{b} are linear with frequency and that the frequency response function (5.22) can be written as

$$G_d(\mathbf{w}) = e^{-j\mathbf{w}d\sqrt{\mathbf{m}\mathbf{e}'}} e^{-\mathbf{w}d\sqrt{\mathbf{m}\mathbf{e}'}\tan \mathbf{d}/2} \quad (5.25)$$

The first exponential represents the delay due to the propagation through d meters of soil. The second exponential represents a linear amplitude distortion introduced by the propagation through the ground. The corresponding IR $g_d(t)$ is found by an inverse Fourier transformation of (5.25) and can be analytically expressed as

$$\begin{aligned} g_d(t) &= \frac{1}{2\mathbf{p}} \int_{-\infty}^{+\infty} G_d(\mathbf{w}) e^{j\mathbf{w}t} d\mathbf{w} \\ &= \frac{1}{2\mathbf{p}} \int_{-\infty}^{+\infty} e^{-\mathbf{a}d} e^{j\mathbf{w}(t-d\sqrt{\mathbf{m}\mathbf{e}'})} d\mathbf{w} \\ &= \frac{d\sqrt{\mathbf{m}\mathbf{e}'(\tan \mathbf{d})}/2}{\mathbf{p}} \left[\frac{1}{2\mathbf{p}} \int_{-\infty}^{+\infty} \frac{\mathbf{p} e^{-\mathbf{w}(d\sqrt{\mathbf{m}\mathbf{e}'(\tan \mathbf{d})}/2)}}{d\sqrt{\mathbf{m}\mathbf{e}'(\tan \mathbf{d})}/2} e^{j\mathbf{w}(t-d\sqrt{\mathbf{m}\mathbf{e}'})} d\mathbf{w} \right] \end{aligned}$$

Hence :

$$g_d(t) = \frac{d\sqrt{\mathbf{m}\mathbf{e}'(\tan \mathbf{d})}/2}{\mathbf{p} \left[(t - d\sqrt{\mathbf{m}\mathbf{e}'})^2 + (d\sqrt{\mathbf{m}\mathbf{e}' \tan \mathbf{d} / 2})^2 \right]} \quad (5.26)$$

The calculation of the IR, characterising a propagation through d meters of soil is made very simple by equation (5.26). As $\tan \mathbf{d}$ and \mathbf{e}' are supposed constant with frequency in the constant Q model, they only have to be measured for one frequency (preferably in the middle of the frequency band of interest).

As an example, we calculate the IR of a wet sandy soil with a moisture content of 10% using (5.26). The real relative permittivity of the soil is $\mathbf{e}'_r = 8.16$ and a loss tangent $\tan \mathbf{d} = 0.085$. Fig. 5-5 shows the impulse response characterising the propagation through a layer of respectively 10 cm and 20 cm of this lossy soil. Fig. 5-6 shows the attenuation and distortion of a transient pulse propagating through the same soil after 10 cm and 20 cm. On the left of the figure (in red), the electric field component of the incoming plane wave is represented. In blue and green the transient pulse is shown at 10 cm and 20 cm in the ground. They are obtained by convolving the incoming pulse (in red) by the IR shown in Fig. 5-5. Both the attenuation in the ground and the dispersive behaviour of the ground, resulting in the broadening of the pulse, are obvious. Note that the decrease in amplitude of the pulse is not due to

spreading loss because a plane wave is assumed. It is only due to the attenuation in the ground.

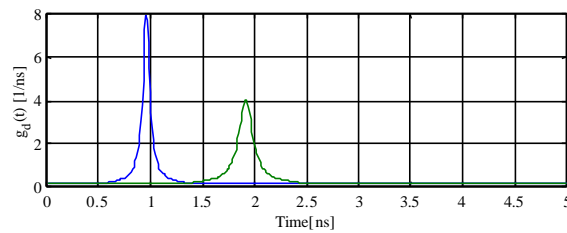


Fig. 5-5: Impulse response of wet sandy soil for $d = 10$ cm (blue) and $d = 20$ cm (green), using (5.26)

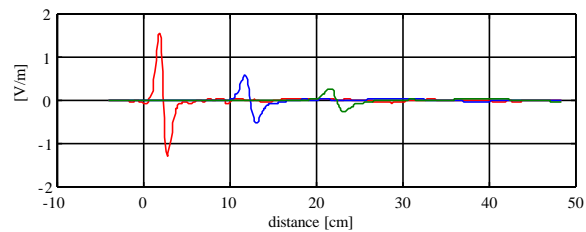


Fig. 5-6: Transient pulse before entering the ground (red) and at 10 cm (blue) and 20 cm (green) in the ground

5.6.4. Impulse Response of objects

General

The IR of an object is defined by the time domain equation (5.9). It can be considered as the time equivalent of the RCS of an object. According to the definition of the RCS in (5.4), that is based on a power ratio of the scattered to the incident field, the IR of an object is based on a ratio of magnitudes of the scattered to incident field. By converting equation (5.9) into the frequency domain, the Frequency Response Function (FRF) of an object, which is defined as the Fourier transform of the IR, can mathematically be expressed, as

$$\Lambda_{1,1}(\vec{a}_i, \vec{a}_s, \mathbf{w}) = 4\mathbf{p} \lim_{R \rightarrow \infty} R \frac{E_s(\vec{a}_s, \mathbf{w})}{E_i(\vec{a}_i, \mathbf{w})} \quad (5.27)$$

with $E_s(\vec{a}_s, \mathbf{w})$ the scattered field in the direction \vec{a}_s

$E_i(\vec{a}_i, \mathbf{w})$ the incoming field on the object from the direction \vec{a}_i .

Hence the IR of an object can be written as

$$\Lambda_{1,1}(\vec{a}_i, \vec{a}_s, t) = \mathfrak{F}^{-1} \left\{ 4\mathbf{p} \lim_{R \rightarrow \infty} R \frac{E_s(\vec{a}_s, \mathbf{w})}{E_i(\vec{a}_i, \mathbf{w})} \right\} \quad (5.28)$$

with \mathfrak{F}^{-1} the inverse Fourier transform.

In (5.27) and (5.28) only one polarisation is assumed. When investigating the complete scattering process of an object, one has to take into account all the polarisations. For an arbitrarily polarised incident plane wave, split into two orthogonal components, the scattered far field can be expressed as

$$\begin{bmatrix} E_s^\perp \\ E_s^\parallel \end{bmatrix} = \begin{bmatrix} S_{1,1} & S_{1,2} \\ S_{2,1} & S_{2,2} \end{bmatrix} \begin{bmatrix} E_i^\perp \\ E_i^\parallel \end{bmatrix} \quad (5.29)$$

or in short

$$\begin{bmatrix} E_s^\perp \\ E_s^\parallel \end{bmatrix} = S \begin{bmatrix} E_i^\perp \\ E_i^\parallel \end{bmatrix} \quad (5.30)$$

where E^\perp is the polarisation normal to the plane of incidence and E^\parallel the polarisation parallel to the plane of incidence. S is called the scattering matrix. The terms $S_{i,j}$ are the scattering coefficients. The subscripts refer to the two orthogonal polarisation components (normal and parallel). The coefficients $S_{1,2}$ and $S_{2,1}$ are the cross-polarisation coefficients. The scattering coefficients are in general complex numbers

and can be represented by an amplitude and phase. The scattering coefficients are directly related to the FRF $\Lambda_{i,j}(\mathbf{w})$ as

$$\Lambda_{i,j}(\mathbf{w}) = 4pR S_{i,j}(\mathbf{w}) \quad (5.31)$$

In the next chapter, the radar range equation will be used to describe a laboratory UWB GPR. In this set-up, the two antennas are placed with a common H-plane, hence the radiated and received field have the same polarisation (normal to the plane of incidence). This means that in the radar range equation we will only use one polarisation. Therefore the subscript i,j in the notation of the IR of the target will be omitted in the future.

RCS and Impulse response of a perfect conductive metallic sphere

As a reference and calibration target in the ground, we often use a metallic sphere. Therefore we discuss its IR in this section. The backscattering on a perfect conductive metallic sphere is given under analytical form by the MIE series [9]. In Fig. 5-7 the RCS of a metallic sphere with a radius of $a = 5$ cm is given as a function of $ka = 2\pi a / \lambda$. The RCS is plotted normalised to the physical cross section of the sphere. In general the RCS of an object is frequency dependent and can be divided into three regions (see Fig. 5-7).

The first region is the *Rayleigh region* or *low frequency region*. In this region the wavelength of the illuminating waveform is large compared to the target dimensions. There is essentially no variation of the phase of the incident wave over the target. The scattered power or the RCS is asymptotically proportional to the fourth power of the frequency.

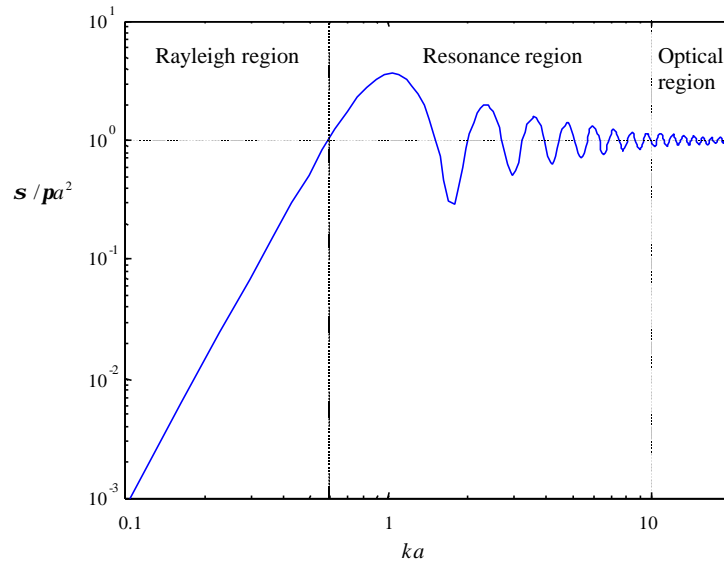


Fig. 5-7: RCS of metallic sphere, showing three scattering regimes

The second region is the *resonance region*. In the resonance region, the incident wavelength is of the order of the size of the target. In this region the RCS of a target can be calculated by solving the integral equation relating the induced current on or in the body to the incident field [2]. Normally these induced currents can be represented as damped sinusoids (see also Chapter 7, Section 7.2.2). The peaks and valleys in the resonance region can be seen as respectively the constructive and destructive interference of different backscattering mechanisms on the target. Fig. 5-8 shows five backscattering mechanisms on a *dielectric sphere* [10]:

1. The specular wave is a return from the front of the sphere
2. The axial wave is due to the reflection on the back of the sphere
3. The glory wave is a wave which is first refracted, then reflected on the back and finally refracted into the backscatter direction; for dielectric targets, this wave can be dominant
4. The stationary wave is also a refracted, reflected and then refracted wave, but its ray paths is not exactly in the backscatter direction
5. The creeping wave is a well known backscatter mechanism that is guided by the curved surface of the sphere.

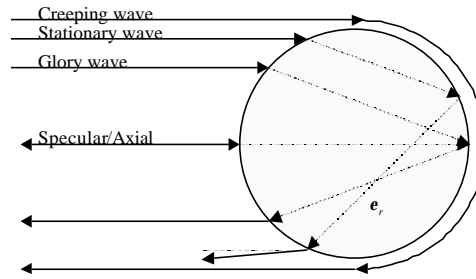


Fig. 5-8: backscattering mechanism on a dielectric sphere

The example of a dielectric sphere is chosen here because in general for dielectric targets there are more scattering mechanisms that interfere. For a metallic sphere, as they are non-penetrable, only the specular wave and the creeping wave interfere. The first resonant peak in the RCS of a metallic sphere (Fig. 5-7) appears for $ka = 1$. This corresponds to the point where one wavelength of the incident wave is exactly equal to the circumference of the sphere. At this frequency, the creeping wave will constructively add to the specular wave in the backscatter direction, hence the peak.

The last region in the RCS is the *optical region*. In this region the target is much larger than the wavelength of the incident field. For a metallic sphere, the RCS in this region converge to a constant value equal to its physical cross section.

In Fig. 5-9 the monostatic impulse response of the metallic sphere (radius $a = 5$ cm) is given. The IR is obtained by (5.28), where the scattered field in the backward direction is calculated using the MIE series. The first reflection (at 3 ns) is the specular reflection on the sphere. The amplitude of this reflection is a function of the cross section of the sphere. In the IR of the metallic sphere, a second reflection appears 0.86 ns later. This reflection is the part of the creeping wave that went around the sphere and scatters in the backward direction. The time between the two reflections is given by

$$\frac{a(2+p)}{c} \quad (5.32)$$

Note that the different backscatter mechanisms can lead to scattering centres that appear further (*i.e.* later in time) than the physical cross diameter of the object. This simple example of the metallic sphere shows very well the correspondence between the IR and the RCS of a target.

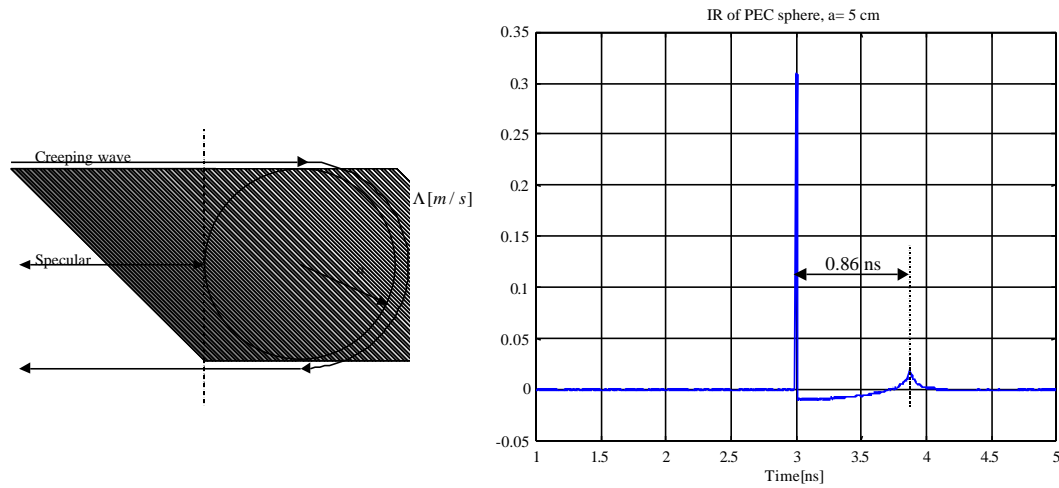


Fig. 5-9: IR of a perfect conductive metallic sphere, showing two scattering centres

In the resonance and optical region, the RCS of the metallic sphere varies around its physical cross section \mathbf{pa}^2 . If we consider as an approximation that this RCS is constant, independent of frequency, then the IR of this fictive target will be a dirac-function. For a radius $a = 5$ cm, hence $\mathbf{s} = \mathbf{pa}^2 = 0.0079$ m², the IR of such a target is calculated as

$$\Lambda(t) = 0,314\mathbf{d}(t) \tag{5. 33}$$

This can also be verified by comparing the definitions of the RCS (5.4) with the definition of the IR (5.28). In the case of a constant RCS, the FRF given by (5.27) is expressed as

$$\Lambda(\mathbf{w}) = \sqrt{4\mathbf{ps}(\mathbf{w})} \tag{5. 34}$$

Hence :

$$\Lambda(t) = \sqrt{4ps}d(t) \quad (5.35)$$

which corresponds with the solution found in (5.33). Comparing the result of (5.33) with the exact IR of a metallic sphere in Fig. 5-7, we see that the amplitude of the dirac-function corresponds with the amplitude of the specular reflection on the sphere. So equation (5.35) can be used as a good approximation for the metallic sphere.

Impulse response of mine-like objects

In general, the response of any arbitrary target can be split into two parts: the early time response and the late time response. The early time is considered to be the scattering response of the object over a time interval, which is of the order of the wave transit time through the object. The late time response contains all the resonances of the target. These resonances are supposed to be little influenced by the orientation of the object and hence contain valuable information for target recognition.

Mine-like targets are non-canonical dielectric or metallic objects. Hence, it is too difficult to calculate analytical solutions of the IR. Numerical calculation methods, like the Finite Difference Time Domain method (FDTD) [11] or the Method of Moments (MoM) [12] are more appropriate.

An alternative way is to measure the IR. In the early stages of this research we did some measurement of the short pulse response on mine like targets. More details on these measurements are found in appendix A and in [13]. The measurements were done with a Time-Domain Scattering Range (TDSR) that was developed at the RMA [14]. The TDSR is designed to study experimentally the transient backscattering of 3D objects. The measurement set-up is schematically represented in Fig. 5-10. The system consists of the following parts. On the transmitting side, a 2 meter long monocone antenna on a square ground plane (3 x 3 m) is coaxially fed by a fast step generator. On the receiving side, a broadband electric field sensor, which is connected to a 20 GHz digitising oscilloscope through a set of UWB low noise amplifiers, detects the transient wave. The 3D Device Under Test (DUT) is put on the ground

plane and is illuminated by the transient spherical wave radiated between the monocone and the ground plane. The backscattering of the DUT is measured by the E-field sensor. Because the long monocone antenna radiates a step function signal and because the electric field sensor is a time derivative sensor, its output yields in fact the *impulse response* of the DUT.

The step generator generates a repetitive step function voltage (10V/45ps) with a high waveform purity. The generator confers to the TDSR a *subcentimeter radial resolution* on the target in the air, which makes it possible to resolve the different scattering centres of the target and to quantify their relative amplitudes.

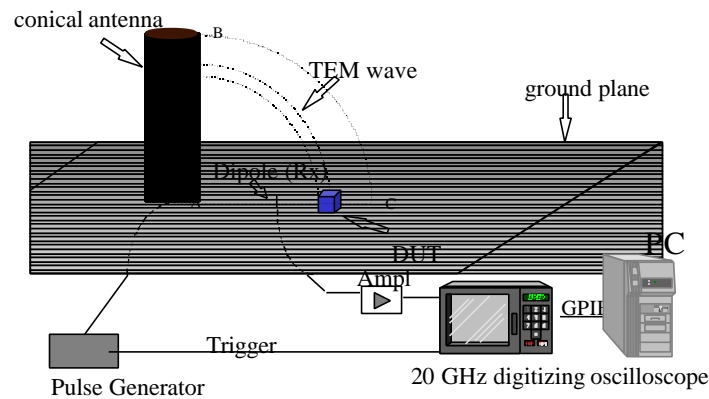


Fig. 5-10: The Time-Domain Scattering Range at the RMA

The Time-Domain Scattering Range is also used to measure the Frequency Response Function (FRF) of non-canonical 3D objects using a dual channel analysis technique. The complete study and conclusions are discussed in appendix A.

Fig. 5-11 shows in blue the measurement of the short pulse response by the TDSR on the Teflon cylinder in free space as a function of time. The Teflon cylinder has the same dimensions as a typical AP mine (8 cm diameter and 3.8 cm thick). For verification, the measured short pulse response of the Teflon cylinders is compared with an FDTD simulation. The simulated data of the short pulse response is represented in red in Fig. 5-11. The result shows that the measurements and the

simulations are very similar, which makes us confident in both approaches. In the late time response of the cylinders, the different scattering centres due to the different backscattering mechanisms clearly appear. In Fig. 5-12 the rays of the specular, axial and creeping waves are represented. The additional travelling time of these paths are also projected on Fig. 5-11, with path 1 as a reference in time. The additional travelling time of path 3 is calculated with the propagation velocity in the Teflon, whereas the additional travelling time of path 4 is calculated with the propagation velocity of free space, hence their difference. The additional travelling time of path 2 gives an indication of the physical size of the target on the time axis. It also indicates the end of the early time response and the beginning of the late time response. The reflections on the back of the Teflon cylinder are small compared to the other backscatter mechanisms.

Just like with the metallic sphere, there are scattering centres, which appear later in time than the reflection on the back of the object. The travelling time of path 2 gives an indication of the physical size of the target on the time axis. There are two scatter centres with larger amplitude that appear later in time than the reflection on the back of the cylinder. This indicates that it will be very difficult to retrieve from the backscattered signal accurate information on the size of the target in the range direction (*cf.* the z direction in Fig. 5-2).

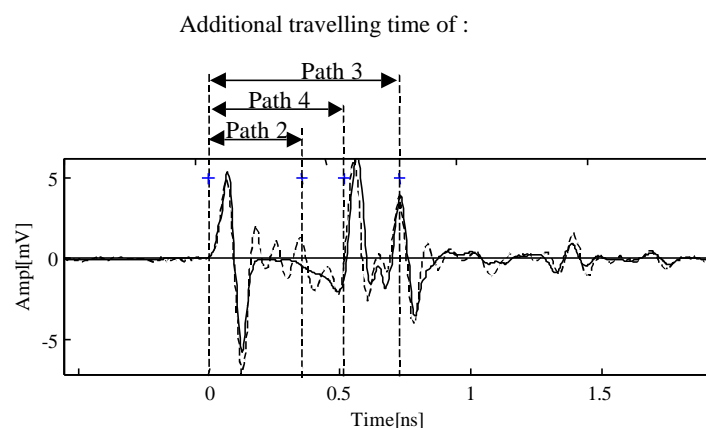


Fig. 5-11: Measured (dashed) and simulated (solid) short pulse response on a Teflon cylinder in free-space. The additional travelling time of path 2,3 and 4 are also represented on the figure.

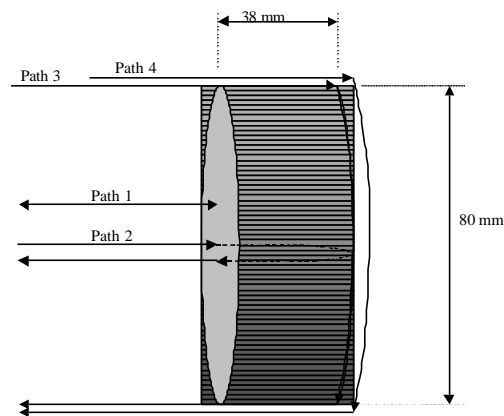


Fig. 5-12: Teflon cylinder with some specific rays

A disadvantage of the above method is that the objects were only considered in free space. In the application of demining, the targets are buried in a lossy half-space. As a consequence the IR of a target will not only depend on the shape and orientation of the target but also on the characteristics of the half-space the target is in. In other words the system to be considered is not the target, but the target in its surrounding medium. In reality the number of unknown parameters influencing the IR will often be too large to accurately forward model an IR of a target, even with numerical models. In the literature, studies are found on the influence of the ground on the late time response of targets [12]. The study is in general very difficult and considered being out of the frame of this research.

5.7. Summary

Using the radar range equation to describe a time domain system has some disadvantages. The radar range equation contains frequency dependent terms and does not take into account the nature of the transmitted signal. Therefore we modelled in this chapter the total system: GPR-ground-target in the time domain by considering it as a cascade of linear responses, resulting in a *time domain GPR range equation* (5.13). The time domain GPR range equation allows us to calculate the received voltage as a function of time at the output of the receiving antenna in terms of the radar characteristics and the target. The model is adapted for the demining

application, *i.e.* antennas off-ground, no multiple layers, etc. The different parts in this cascade are the pulse generator, the antennas modelled by their normalised impulse response, the spreading losses, the transmission coefficients on the air-ground interface, the propagation through the ground and the scattering on the target in the ground. Fig. 5-13 shows a schematic representation of the different parts of the time domain GPR range equation, summarising the whole chapter. The GPR configuration is as shown in Fig. 5-2 and the target is a metallic sphere with a radius of 5 cm. The influence of each part in the cascade on the signal is visualised.

For the characterisation of the losses in the ground, an analytical expression of the impulse response modelling the propagation in the ground is presented. The expression of the impulse response is calculated from the theoretical frequency response function of the lossy soil and takes into account the attenuation and the dispersive behaviour of the ground. The only three parameters in this expression are the real part of the permittivity, the loss tangent (which are both considered as being independent of frequency for a given soil type and moisture content) and the path length in the ground.

The targets in the ground are also characterised by an IR. We calculated and discussed the exact IR of a metallic sphere and the measured short pulse response of a Teflon cylinder in free space. We showed that the IR is a combination of different scattering mechanism. In general we can say that the dimensions of the targets are of the same order as the wavelengths used in the GPR. This means that we are primarily working in the resonance region of the scattering, leading to scattering centres that appear later in time than the reflection on the back of the target.

In the next chapter we will use the time domain GPR range equation to study and optimise the performance of a laboratory UWB GPR system.

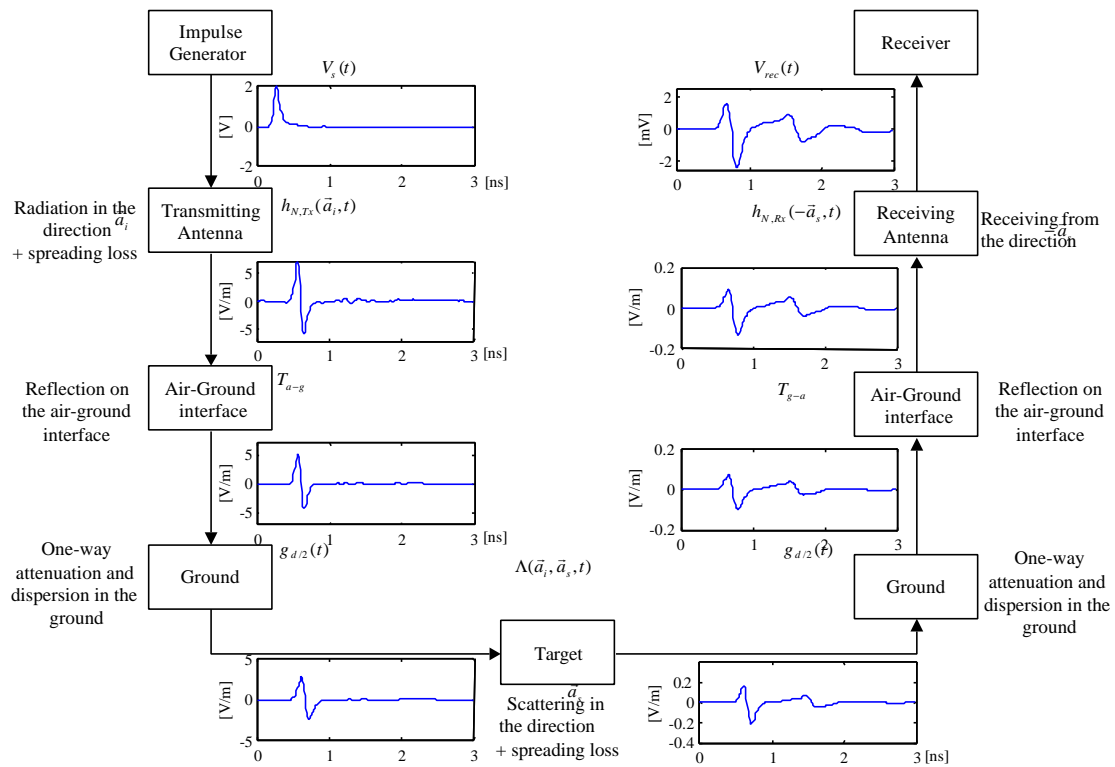


Fig. 5-13: Schematic representation of the different parts of the time domain GPR range equation

REFERENCES

- [1] M. Skolnik, *Radar handbook*. New York: McGraw-Hill, 1990.
- [2] M. L. Van Blaricum, *Introduction to Ultra-Wideband Radar Systems*. J. D. Taylor, Ed., USA: CRC Press, 1995, ch. 9.
- [3] J. L. Davis and A. P. Annan, "Ground-Penetrating Radar for High-Resolution Mapping of Soil and Rock Stratigraphy," *Geophysical Prospecting*, vol. 37, pp. 531-551, 1998.
- [4] B. Scheers, Y. Plasman, M. Piette, M. Acheroy and A. Vander Vorst, "Laboratory UWB GPR system for landmine detection," *Eight International Conference on Ground Penetrating Radar*, Gold Coast, Australia, pp. 747-752, May 2000.
- [5] J. Stratton, *Electromagnetic Theory*. New York: McGraw-Hill, 1941.
- [6] F. Lehmann, "Fresnel equations for reflection and transmission at boundaries between two conductive media, with applications to georadar problems," *6th International Conference on Ground Penetrating Radar (GPR96)*, Japan, pp. 555-559, Sep.-Oct. 1996.
- [7] M. Storme, I. Huynen and A. Vander Vorst, "Characterization of wet soils in the 2-18 GHz frequency range," *Microwave and optical technology letters*, vol. 21, no. 5, June 1999.
- [8] J. Mast and E. Johansson, "Three-dimensional ground penetrating radar imaging using synthetic aperture time domain focusing," *Spie Proceedings on advanced microwave and millimeterwave detectors*, vol. 2275, pp. 205-214, Jul. 1994.
- [9] G. Mie, "Beitrage zur Optik trüber Medien, speziell kolloidaler Metallösungen," *Ann. Physik.*, band 25, pp. 377-445, March 1908.
- [10] S. R. Cloude, A. Milne, C. Thornhill and G. Crisp, "UWB SAR detection of dielectric targets," *IEE Eurel International Conference on The Detection of Abandoned Land Mines*, Edinburgh, UK, pp. 114-118, Oct. 1996.
- [11] K. S. Kunz and R. J. Luebbers, *The finite Difference Time Domain Method for Electromagnetics*. London: CRC Press , 1993.
- [12] S. Vitebskiy and L. Carin, "Resonances of Perfectly Conducting Wires and Bodies of Revolution Buried in a Lossy Dispersive Half-Space," *IEEE Trans. on Antennas and Propagat.*, vol. 44, no. 12, pp. 1575-1583, Dec. 1996.

- [13] B. Scheers and M. Piette, "Short-pulse response of antipersonnel landmines to UWB GPR signals", *Seventh International Conference on Ground Penetrating Radar*, Kansas, USA, pp. 337-341, May 1998.
- [14] M. Piette, *Banc de mesure en régime transitoire de la signature radar d'objets tridimensionnels*, Doctoral thesis, Université catholique de Louvain and Royal Military Academy, Belgium, Oct. 1995.

